



**HAL**  
open science

# Lattice Boltzmann Simulation of Asymptotic Longitudinal Mass Dispersion in Reconstructed Random Porous Media

Chen Yang, Yixiong Lin, Gérald Debenest, Akira Nakayama, Ting Qiu

► **To cite this version:**

Chen Yang, Yixiong Lin, Gérald Debenest, Akira Nakayama, Ting Qiu. Lattice Boltzmann Simulation of Asymptotic Longitudinal Mass Dispersion in Reconstructed Random Porous Media. *AICHE Journal*, 2018, vol. 00 (n° 00), pp. 1-11. 10.1002/aic.16088 . hal-01803146

**HAL Id: hal-01803146**

**<https://hal.science/hal-01803146v1>**

Submitted on 30 May 2018

**HAL** is a multi-disciplinary open access archive for the deposit and dissemination of scientific research documents, whether they are published or not. The documents may come from teaching and research institutions in France or abroad, or from public or private research centers.

L'archive ouverte pluridisciplinaire **HAL**, est destinée au dépôt et à la diffusion de documents scientifiques de niveau recherche, publiés ou non, émanant des établissements d'enseignement et de recherche français ou étrangers, des laboratoires publics ou privés.




## Open Archive TOULOUSE Archive Ouverte (OATAO)

OATAO is an open access repository that collects the work of Toulouse researchers and makes it freely available over the web where possible.

This is an author-deposited version published in : <http://oatao.univ-toulouse.fr/>  
Eprints ID : 19828

**To link to this article** : DOI:10.1002/aic.16088

URL : <https://doi.org/10.1002/aic.16088>

**To cite this version** : Yang, Chen and Lin, Yixiong and Debenest, Gérald  and Nakayama, Akira and Qiu, Ting *Lattice Boltzmann Simulation of Asymptotic Longitudinal Mass Dispersion in Reconstructed Random Porous Media*. (2018) AICHE Journal, vol. 00 (n° 00). pp. 1-11. ISSN 0001-1541

Any correspondence concerning this service should be sent to the repository administrator: [staff-oatao@listes-diff.inp-toulouse.fr](mailto:staff-oatao@listes-diff.inp-toulouse.fr)

# Lattice Boltzmann Simulation of Asymptotic Longitudinal Mass Dispersion in Reconstructed Random Porous Media

Chen Yang and Yixiong Lin

Fujian Universities Engineering Research Center of Reactive Distillation Technology, College of Chemical Engineering, Fuzhou University, Fuzhou 350116, Fujian, China

Gérald Debenest

Université de Toulouse, INPT, UPS, IMFT (Institut de Mécanique des Fluides de Toulouse), 31400 Toulouse, France

Akira Nakayama

Dept. of Mechanical Engineering, Shizuoka University, 3-5-1 Johoku, Nakaku, Hamamatsu 432-8561, Japan

School of Civil Engineering and Architecture, Wuhan Polytechnic University, Wuhan 430023, Hubei, China

Ting Qiu 

Fujian Universities Engineering Research Center of Reactive Distillation Technology, College of Chemical Engineering, Fuzhou University, Fuzhou 350116, Fujian, China

*To research macroscopic mass transport characteristics of porous media, a lattice Boltzmann method (LBM) approach was utilized to calculate asymptotic longitudinal mass dispersion. In this study, a D2Q9 model with multi-relaxation-time (MRT) collision operator, which is appropriate for incompressible flow with a high Péclet number without refining the lattice, was chosen. With respect to the microstructure of porous media, random placement (RP) method was applied to obtain randomly positioned particles. Based on the exhausted numerical results presented in the study, a new correlation of longitudinal mass dispersion was established. By comparing with available experimental data in the literature, reasonable agreements are observed in a wide porosity range from 0.3 to 0.7, indicating the validity of the proposed correlation.*

*Keywords: LBM, multirelaxation-time, longitudinal mass dispersion, random placement, porous media*

## Introduction

The processes of mass transport in porous media are subjects of remarkably practical importance in fields of chemical engineering and environment. To describe the mass transport processes in porous media, the macroscopic continuum equation obtained using the method of volume averaging<sup>1-3</sup> is commonly used by many researchers<sup>4-11</sup> due to its convenience and efficiency. Prior to that, one should obtain the effective diffusivity that plays an important role in solving the macroscopic continuum equation. As pointed out by Chai et al.,<sup>12</sup> three methods that are analytical or semianalytical method, experimental method, and numerical method, respectively, are applicable to determine the effective diffusivity. As the limitations of the first two methods, such as extension difficulties in complicated structures and insufficiency in provided information, numerical method has been extensively applied in the literature.

With respect to numerical method, there are two approaches. The first one is the computational fluid dynamics (CFD) approach, which requires an accurate description of the pore structure and the discretization of the model into pore and solid phases, so that the microscopic equations can be solved in the pore spaces with appropriate conditions applied at the pore and solid interfaces. In reality, however, it is difficult to specify boundary values, and unstructured or block structured meshes are required to represent the complex pathways due to the existence of arbitrarily complex solid matrix. To overcome these shortcomings of the conventional approach, lattice Boltzmann method (LBM) approach uses a mesoscopic equation to determine macroscopic transport properties. As affirmed by extensive studies,<sup>13-20</sup> LBM has the advantages of simplicity of programming, inherent parallelism and ease in dealing with a complex boundary. Wang et al.<sup>21</sup> proposed a corrected heat flux of the thermal lattice Boltzmann model to calculate the effective thermal conductivity of porous media with multiphase. The solid matrix of porous media was generated by the quartet structure generation set (QSGS).<sup>22</sup> To evaluate the volatile organic compounds emission or sorption characteristics in porous building materials,

Hussain et al.<sup>23</sup> utilized LBM to obtain effective diffusion coefficient. Moreover, a novel numerical random generation macromeso pores (RGMMP) method was proposed to represent geometrical and morphological information of porous building materials. By comparing with available experimental data, it has been found that the predicted effective diffusion coefficients exhibit acceptable accuracy. For the purpose of effective diffusivity prediction of porous media, Chai et al.<sup>12</sup> conducted a comparative study on two lattice Boltzmann models, which are BGK model and multi-relaxation-time (MRT) model, respectively. The comparison results indicated that the MRT model is more appropriate to investigate diffusion in porous media than BGK model.

Nevertheless, it should be mentioned that in the above-referenced studies related to effective diffusivity of porous media, effect of dispersion was not investigated. Moreover, solid matrix of porous media was assumed to be impermeable. Hence, it can be concluded that only tortuosity which represents the effect of interconnected pore space on the effective conductivity was evaluated. It is well known that, however, dispersion is more important than tortuosity when fluid flow occurs in porous media. By analytically analyzing macroscopic mass transport processes in porous media with randomly positioned permeable particles, Koch and Brady<sup>24</sup> firstly proposed that mass dispersion embraces three counterparts, which are mechanical dispersion, boundary-layer dispersion and holdup dispersion, respectively. Holdup dispersion is also known as the active dispersion. This appears when transport phenomenon occurs not only in the fluid phase but in several phases.<sup>4</sup> Furthermore, the full form of the longitudinal mass dispersion at high Péclet numbers was obtained, which was validated by comparing with experimental data for the case of fixed beds with impermeable particles and  $\varepsilon=0.5$ . For different porosities, Maier et al.<sup>25</sup> and Kandhai et al.<sup>26</sup> performed nuclear magnetic resonance (NMR) spectroscopy experiments to obtain the asymptotic longitudinal mass dispersion of fixed beds with  $\varepsilon=0.44$  and  $\varepsilon=0.37$ , respectively. But it has been found that the coefficients in the full form of the longitudinal mass dispersion correlated from experimental data of Maier et al.<sup>25</sup> and Kandhai et al.<sup>26</sup> are not consistent with that of Koch and Brady.<sup>24</sup> Due to the significant importance of mass dispersion, it is worth revisiting the mass transport phenomena in porous media with a wide range of porosity.

In this study, we would like to apply a LBM approach to investigate the fluid flow and mass transport in porous media with randomly positioned permeable particles. In this approach, a D2Q9 model with multi-relaxation-time (MRT) collision operator that is appropriate for incompressible flow with a high Péclet number without refining the lattice is chosen. Moreover, LBM approach validation is conducted by comparing with available experimental data. Based on the LBM approach, effects of various parameters associated with mechanical dispersion, boundary-layer dispersion and holdup dispersion are investigated, so as to obtain a general correlation of asymptotic longitudinal mass dispersion that is valid in a wide range of porosity.

## Lattice Boltzmann Method for Fluid Flow and Mass Transfer Equations

In this study, we discuss convective mass transfer phenomenon in porous media. In order to explain mass transfer process, a schematic diagram is illustrated in Figure 1. Porous media is composed of the void and solid matrix that is also

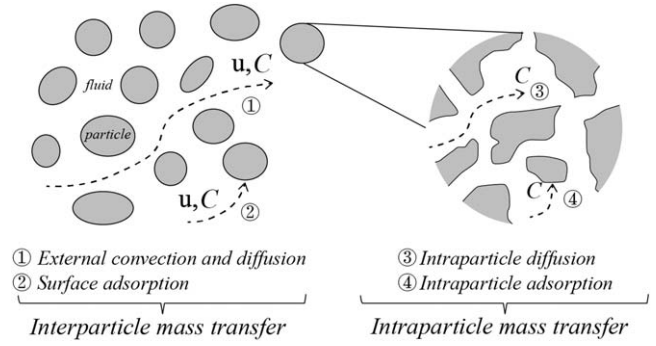


**Figure 1. Schematic diagram of mass transfer in porous media.**

microporous. Thus, they are permeable and a transport equation is specified within this region. Then, mass transfer in porous media contains two counterparts, which are interparticle mass transfer and intraparticle mass transfer, respectively. The interparticle mass transfer occurs in the void of porous media, which includes the external diffusion, convection and surface adsorption, while the intraparticle mass transfer takes place inside the catalyst particles, which includes the intraparticle diffusion and intraparticle adsorption.

Based on the description of convective mass transport of porous media with permeable catalyst particles, the governing equations for the mass transfer system without chemical reactions of mass, momentum and solute concentration are expressed as follows

$$\frac{\partial \rho}{\partial t} + \nabla \cdot (\rho \mathbf{u}) = 0 \quad \text{in } V \quad (1)$$

$$\frac{\partial (\rho \mathbf{u})}{\partial t} + \nabla \cdot (\rho \mathbf{u} \mathbf{u}) = -\nabla p + \nabla \cdot \boldsymbol{\sigma} \quad \text{in } V_f \quad (2)$$

$$\frac{\partial C}{\partial t} + \nabla \cdot (C \mathbf{u}) = \nabla \cdot (D \nabla C) \quad \text{in } V \quad (3)$$

where  $\rho$  is the local mass density;  $\mathbf{u}$  is the fluid velocity tensor;  $p$  is the pressure; and  $\boldsymbol{\sigma}$  is the viscous stress tensor;  $C$  is the solute concentration;  $D$  is the related diffusion coefficient.  $V$  is the total volume, whereas  $V_f$  is the fluid volume around catalyst particles.

On the catalyst particles surface, Koch and Brady<sup>24</sup> used the continuity of flux and solubility conditions that are indicated as follows

$$D_f \mathbf{n} \cdot \nabla C_{\text{out}} = D_p \mathbf{n} \cdot \nabla C_{\text{in}} \quad (4)$$

$$C_{\text{out}} = m C_{\text{in}} \quad (5)$$

where  $D_f$  and  $D_p$  are, respectively, the molecular diffusivity of the solute outside the catalyst particles and intraparticle diffusivity of the solute inside the catalyst particles;  $\mathbf{n}$  is the normal unit vector from the catalyst particle surfaces to the fluid;  $m$  is the ratio of the solubilities of the solute in the fluid and in the catalyst particles;  $C_{\text{out}}$  and  $C_{\text{in}}$  are the concentrations in the void and in the catalyst particles, respectively.

## Lattice Boltzmann solver for fluid flow equation

Lattice Boltzmann equation can be decomposed into two parts: collision and streaming, the collision and streaming steps are defined as follows:

$$\text{Collision step : } f_i^*(\mathbf{x}, t) = f_i(\mathbf{x}, t) - \Omega [f_i(\mathbf{x}, t) - f_i^{\text{eq}}(\mathbf{x}, t)] \quad (6)$$

$$\text{Streaming step : } f_i(\mathbf{x} + \mathbf{e}_i \Delta t, t + \Delta t) = f_i^*(\mathbf{x}, t) \quad (7)$$

where  $f_i(\mathbf{x}, t)$  is the distribution function associated with the discrete velocity  $\mathbf{e}_i$  at position  $\mathbf{x}$  and time  $t$ ;  $f_i^{\text{eq}}(\mathbf{x}, t)$  is equilibrium distribution function;  $f_i^*(\mathbf{x}, t)$  is the post-collision distribution function;  $\Omega$  is the collision operator.

Based on the collision operator, the model of the lattice Boltzmann equation can be classified into three kinds, that is, the Bhatnagar-Gross-Krook (BGK) model or single-relaxation-time (SRT) model,<sup>27–30</sup> the two-relaxation-time (TRT)<sup>31,32</sup> and multiple-relaxation-time (MRT) models.<sup>33,34</sup> In this work, the multiple-relaxation-time (MRT) model was chosen because its advantages in numerical stability, accuracy, and computational efficiency.<sup>34</sup> The MRT collision operator is given by

$$f_i(\mathbf{x} + \mathbf{e}_i \Delta t, t + \Delta t) - f_i(\mathbf{x}, t) = -(\mathbf{M}^{-1} \mathbf{S}_f \mathbf{M}) [f_i(\mathbf{x}, t) - f_i^{\text{eq}}(\mathbf{x}, t)] \quad (8)$$

where  $\mathbf{M}$  is the transformation matrix;  $\mathbf{S}_f$  is a diagonal relaxation matrix. Considering the accuracy of the results, we select D2Q9 discrete velocities model to establish the hydrodynamics model as seen in Figure 2. For the D2Q9 discrete velocities model, we can define

$$\mathbf{e}_i = \begin{cases} (0, 0) & i=0 \\ \left\{ \cos \left[ (i-1) \frac{\pi}{2} \right], \sin \left[ (i-1) \frac{\pi}{2} \right] \right\} & i=1, 2, 3, 4 \\ \sqrt{2} \left\{ \cos \left[ (i-5) \frac{\pi}{2} + \frac{\pi}{4} \right], \sin \left[ (i-5) \frac{\pi}{2} + \frac{\pi}{4} \right] \right\} & i=5, 6, 7, 8 \end{cases} \quad (9)$$

$$\mathbf{M} = \begin{bmatrix} 1 & 1 & 1 & 1 & 1 & 1 & 1 & 1 & 1 \\ -4 & -1 & -1 & -1 & -1 & 2 & 2 & 2 & 2 \\ 4 & -2 & -2 & -2 & -2 & 1 & 1 & 1 & 1 \\ 0 & 1 & 0 & -1 & 0 & 1 & -1 & -1 & 1 \\ 0 & -2 & 0 & 2 & 0 & 1 & -1 & -1 & 1 \\ 0 & 0 & 1 & 0 & -1 & 1 & 1 & -1 & -1 \\ 0 & 0 & -2 & 0 & 2 & 1 & 1 & -1 & -1 \\ 0 & 1 & -1 & 1 & -1 & 0 & 0 & 0 & 0 \\ 0 & 0 & 0 & 0 & 0 & 1 & -1 & 1 & -1 \end{bmatrix} \quad (10)$$

And the equilibrium distribution function with D2Q9 model proposed by He and Luo<sup>35</sup> for the incompressible Navier-Stokes equation can be given by

$$f_i^{\text{eq}}(\mathbf{x}, t) = w_i \left\{ \rho + \rho_0 \left[ \frac{\mathbf{e}_i \cdot \mathbf{u}}{c_s^2} + \frac{(\mathbf{e}_i \cdot \mathbf{u})^2}{2c_s^4} - \frac{\mathbf{u}^2}{2c_s^2} \right] \right\} \quad (11)$$

where  $w_i$  is the weight coefficient;  $c_s$  is the lattice sound speed. Moreover,  $\rho$  is a variable related to the pressure as  $p = c_s^2 \rho$ , while  $\rho_0$  denotes the density of fluid, which is constant. For D2Q9 model, we choose  $w_i$  and  $c_s$  as follows, according to<sup>35</sup>

$$w_0 = \frac{4}{9}, w_{1-4} = \frac{1}{9}, w_{5-8} = \frac{1}{36}, c_s = \frac{1}{\sqrt{3}} \quad (12)$$

Moreover, the relaxation matrix  $\mathbf{S}_f$  for D2Q9 is indicated as follow

$$\mathbf{S}_f = \text{diag}(s_\rho, s_e, s_e, s_j, s_q, s_j, s_q, s_v, s_v) \quad (13)$$

Note that the parameters  $s_i$  in the relaxation matrix are normally in the range of 0 to 2. As suggested by Lallemand and

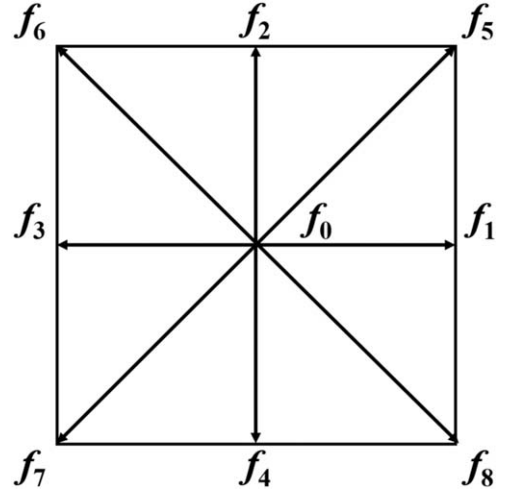


Figure 2. D2Q9 discrete velocities model for fluid flow.

Luo,<sup>33</sup> Luo et al.,<sup>34</sup> Bettaibi et al.,<sup>36</sup> and Zhou et al.,<sup>16</sup> values of the relaxation parameters in Eq. 13 are set as follows

$$s_\rho = s_j = 1.0, s_e = s_e = s_v = \frac{1}{\tau_f}, s_q = \frac{16s_v - 8}{8s_v - 1} \quad (14)$$

where  $\tau_f$  is the relaxation time and equal to 1.0, since it can achieve optimal stability according to previous studies. Moreover, through the Chapman-Enskog expansion, the relaxation rate  $s_v$  can be converted to macroscopic kinematic viscosity  $\nu$  and the macroscopic density and velocity can be given by the following equations

$$\nu = c_s^2 \left( \frac{1}{s_v} - \frac{1}{2} \right) \Delta t \quad (15)$$

$$\rho = \sum_{i=0}^8 f_i(\mathbf{x}, t) \quad (16)$$

$$\rho \mathbf{u} = \sum_{i=0}^8 f_i(\mathbf{x}, t) \mathbf{e}_i \quad (17)$$

### Lattice Boltzmann solver for mass transfer equation

The Bhatnagar-Gross-Krook (BGK) model is the most widely used model for mass transfer. As pointed out in numerous previous studies, however, the numerical accuracy and stability of BGK model depend strongly on the relaxation time in the evolution equation (Holme and Rothman,<sup>37</sup> Sterling and Chen,<sup>38</sup> Rakotomalala et al.,<sup>39</sup> Leconte et al.<sup>40</sup>) The relaxation time for the convection-diffusion equation is determined by the diffusion coefficient. In the lattice Boltzmann equation, the relaxation time of the solute concentration distribution function equation is

$$\tau_g = \frac{D}{c_s^2 \Delta t} + 0.5 = \frac{Ma}{Pe} \frac{L}{c_s \Delta t} + 0.5 \quad (18)$$

where  $Ma = \frac{U}{c_s}$  and  $Pe = \frac{UL}{D}$  are the Mach number and the Péclet number, respectively. Moreover,  $U$  and  $L$  are respectively the characteristic velocity and the reference length. As indicated in Eq. 18, it can be easily deduced that  $\tau_g$  approaches to 0.5 with the increase of  $Pe$ , resulting in numerical instability problem as pointed out by Sterling and Chen.<sup>38</sup> In order to improve the stability, one can use a large number of  $L$ . But this will require to refine the lattice. Hence, it would cost massive

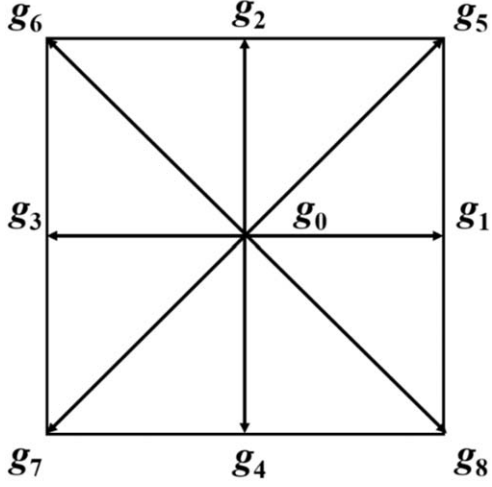


Figure 3. D2Q9 discrete velocities model for mass transfer.

computer resources and significantly reduce the computational efficiency. In the literature, the multiple-relaxation-time (MRT) model was proposed to solve the instability problem without refining the lattice. The evolution equation of the MRT model for the convection-diffusion equation is presented as below

$$g_i(\mathbf{x} + \mathbf{e}_i \Delta t, t + \Delta t) - g_i(\mathbf{x}, t) = -(\mathbf{M}^{-1} \mathbf{S}_g \mathbf{M}) [g_i(\mathbf{x}, t) - g_i^{eq}(\mathbf{x}, t)] \quad (19)$$

where  $\mathbf{S}_g$  is a diagonal relaxation matrix for mass transfer. As seen in Figure 3, D2Q9 discrete velocities model is selected. Moreover, the equilibrium distribution function with D2Q9 model can be given by

$$g_i^{eq}(\mathbf{x}, t) = w_i C \left[ 1 + \frac{\mathbf{e}_i \cdot \mathbf{u}}{c_s^2} + \frac{(\mathbf{e}_i \cdot \mathbf{u})^2}{2c_s^4} - \frac{\mathbf{u}^2}{2c_s^2} \right] \quad (20)$$

For mass transfer, the relaxation matrix  $\mathbf{S}_g$  for D2Q9 is indicated as follow

$$\mathbf{S}_g = \text{diag}(\lambda_0, \lambda_1, \lambda_2, \lambda_3, \lambda_4, \lambda_5, \lambda_6, \lambda_7, \lambda_8) \quad (21)$$

where the relaxation parameters in Eq. 21 are taken as  $\lambda_0 = 1.0$ ,  $\lambda_1 = \lambda_2 = 1.1$ ,  $\lambda_3 = \lambda_4 = \lambda_5 = \lambda_6 = 1/\tau_g$ , and  $\lambda_7 = \lambda_8 = 1.2$ , which are the same as Meng and Guo.<sup>41</sup> Moreover, the macroscopic concentration  $C$  is calculated by the conservation law

$$C = \sum_{i=0}^8 g_i \quad (22)$$

### Boundary conditions for fluid flow and mass transfer

For hydrodynamic boundary conditions, the periodic boundary conditions used by Succi<sup>42</sup> are applied to inlet and outlet boundaries. The expressions of LBM are as follows

$$f_{1,5,8}(0, j) = f_{1,5,8}(N_x - 1, j) \quad (23a)$$

$$f_{3,6,7}(N_x, j) = f_{3,6,7}(1, j) \quad (23b)$$

where  $N_x$  stands for the sum of lattices in the  $x$  dimension, and  $j$  corresponds to the indices for the  $y$  dimension. For mass transfer boundary conditions, however, the Dirichlet boundary conditions are applied to inlet and outlet boundaries. Therefore, the non-equilibrium extrapolation scheme proposed by Guo et al.<sup>43</sup> was used and given by

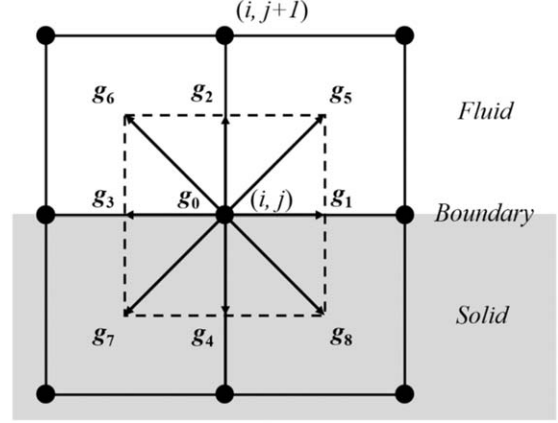


Figure 4. Concentration distribution on a fluid-solid boundary of D2Q9 lattice.

$$g_{1,5,8}(0, j) = g_{1,5,8}^{eq}(0, j) + [g_{1,5,8}(1, j) - g_{1,5,8}^{eq}(1, j)] \quad (24a)$$

$$g_{3,6,7}(N_x, j) = g_{3,6,7}^{eq}(N_x, j) + [g_{3,6,7}(N_x - 1, j) - g_{3,6,7}^{eq}(N_x - 1, j)] \quad (24b)$$

In this work, we investigate both permeable and non-permeable particles. For impermeable particles, the boundary model proposed by Kang et al.<sup>44</sup> and Kang et al.,<sup>45</sup> which strictly ensures solute mass conservation in the above process, was utilized. In terms of the corresponding concentration and its gradient, the concentration distribution functions are presented as follow

$$\sum_i g_i \mathbf{e}_i = C \mathbf{u} - D \nabla C \quad (25)$$

As shown in Figure 4, the concentration distribution functions on a static fluid-solid boundary node  $(i, j)$  under the D2Q9 model are illustrated. After streaming process of the lattice Boltzmann equation, the concentration distribution functions  $g_4$ ,  $g_7$ , and  $g_8$  corresponding to boundary node are known, but  $g_2$ ,  $g_5$ , and  $g_6$  entering the fluid domain in the next streaming step are unknown. So, we apply Eqs. 26 to obtain the unknown concentration distribution functions. The unknown concentration distribution functions can be given by

$$g_2(i, j) = 2/9C(i, j) - g_4(i, j) \quad (26a)$$

$$g_5(i, j) = 1/18C(i, j) - g_7(i, j) \quad (26b)$$

$$g_6(i, j) = 1/18C(i, j) - g_8(i, j) \quad (26c)$$

With regard to permeable particles, the mass transport process occurs not only outside the particles, but also in the interior of the particles. Throughout the process, the bulk fluid solute concentration is transferred to the surface of the particles, in the form of convection and diffusion, and then, the solute diffuses into the particles. Nevertheless, the difficulty is the treatment of the discontinuity of the solute concentration across the interface, as indicated in Eq. 5. In this case, the concentration transformation method first proposed by Yang and Mao<sup>46</sup> was used to make the concentration field continuous across the interface.

## Physical Geometry and Code Validation

### Reconstruction of porous media

To implement the lattice Boltzmann model to investigate mass transport phenomenon in porous media, the suitable discretized geometry of porous media should be obtained in

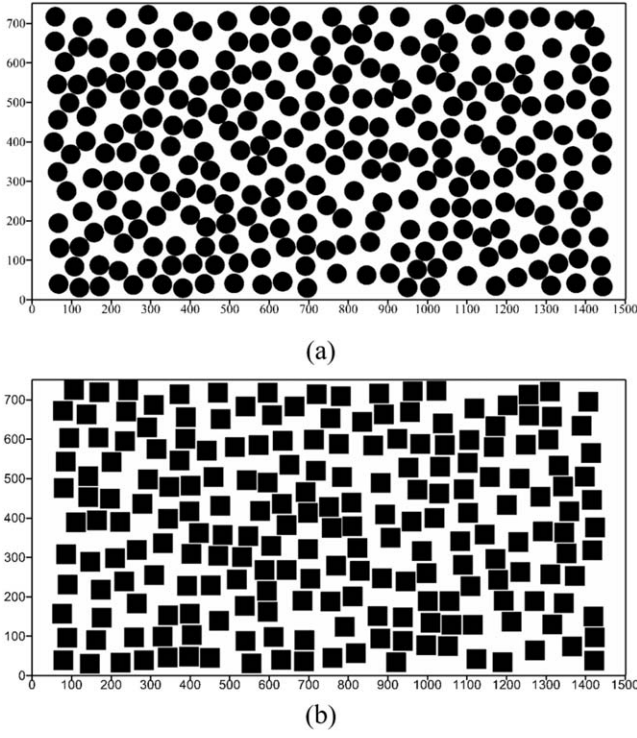


**Figure 5. Reconstructed microstructure of porous media with porosity of 0.5: (a) circular cylinders; (b) square cylinders.**

advance. For most porous media, it is possible to acquire its real experimental images by imaging techniques such as computed tomography (CT),<sup>13</sup> magnetic resonance imaging (MRI).<sup>47,48</sup> However, the numerical solutions based on these experimental images are only valid for specific porous media structures. Moreover, experimental measurements usually require many carefully controlled experiments and are normally expensive,<sup>49</sup> even if HPC (High Performance Computing) techniques allow to deal with this issue. Instead of using the experimental images, many researchers developed mathematical algorithm to reconstruct microstructures of porous media since many decades.<sup>50</sup> The results indicated that the predictions of macroscopic properties are in good agreement with experimental data. With respect to the microstructure of the packed bed that consists of abundant randomly distributed catalyst particles, Yazdchi et al.<sup>51</sup> compared four different algorithms to generate random, nonoverlapping particle arrays, which are random placement (RP), Monte Carlo (MC) procedure, energy minimization (EM) approach and molecular dynamic (MD) simulations, respectively. Pair distribution function was used to characterize and classify the difference of microstructures. It has been found that random placement can get similar trend of pair distribution and have the same permeability by comparing with Monte Carlo procedure and molecular dynamic simulations. To avoid correlation effects observed when the simulation domain is too small,<sup>52</sup> the domain with dimension  $1500 \times 750$  (with particles of diameter 50 lattice points) was used in the study. The longest dimension is along the macroscopic flow direction in our simulations. We utilize MATLAB programming software to realize random placement algorithm, so as to reconstruct the packed bed microstructure.

As shown in Figure 5, random placement algorithm was applied to generate porous media with circular and square

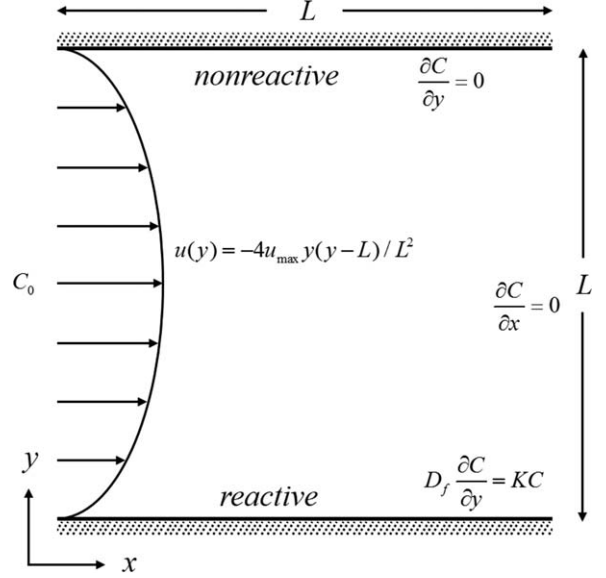


**Figure 6. Schematic diagram of convection-diffusion system based on L ev esque solution.**

cylinders at the same porosity of 0.5. It should be mentioned that the curved boundaries of circular cylinders were approximated by the zigzag lines. This approximation has been extensively used in complex geometries to make lattice Boltzmann model more efficient. In terms of lattice Boltzmann method, Chai et al.<sup>12</sup> discussed the diffusion process of square and circular cylinders in a square arrangement. Both numerical and experimental results indicated that under the same porosity, effective diffusivity of square cylinders in a square arrangement is quite close to that of circular cylinders in a square arrangement. Furthermore, since a large number of lattices are needed to deal with curved boundary, square cylinders are chosen to perform simulations in this study.

#### Verification example

Before the code validation, a benchmark example related to mass transfer problem based on L ev esque solution<sup>53</sup> was conducted to compare the results obtained by the LBM approach with the analytical prediction. As illustrated in Figure 6, a parabolic velocity of fully developed laminar flow is applied for the entire domain, and is written as

$$u(y) = -4u_{\max} y(y-L)/L^2 \quad (27)$$

where  $u_{\max}$  is the axial velocity. For the inlet and outlet boundary conditions, constant concentration  $C_0$  and zero-flux condition are imposed, respectively. Moreover, the upper surface is set to be nonreactive with a zero-flux condition. And the first-order Henry's adsorption process is applied in the bottom boundary

$$D_f \frac{\partial C}{\partial y} = KC \quad (28)$$

where  $K$  is Henry's law constant.

In this work, we use the MRT model with D2Q9 and D2Q5 discrete velocities models to calculate the steady-state normalized mass flux  $\bar{Q}$  at the bottom for the above mass transfer process and compare it with the L ev esque solution. The L ev esque solution obtained by L ev esque<sup>53</sup> and Machado<sup>54</sup> is expressed as

**Table 1. Simulation Parameters for Convection-Diffusion System with Surface Adsorption Process**

$L$	$C_0$	$u_{\max}$	$D_f$	$K$	$Pe$
100	1.0	0.003	0.005	1.0	40
100	1.0	0.03	0.005	1.0	400
100	1.0	0.06	0.005	1.0	800

$$\bar{Q} = \frac{L}{C_0} \frac{\partial C}{\partial n} = 0.854 \left( \frac{u_{\max} L^2}{x D_f} \right)^{\frac{1}{3}} \quad (29)$$

where  $x$  is the stream wise coordinate. The relevant simulation parameters under lattice units are presented in Table 1. As shown in Figure 7, it can be clearly seen that by comparing with the Lévêque solution, D2Q9 discrete velocities model exhibits better agreement than D2Q5 discrete velocities model, varying the Péclet number. Therefore, we select D2Q9 discrete velocities model to simulate mass transfer process in this study.

### Code validation

The model in this section is validated by longitudinal dispersion coefficient, which can be calculated by the method developed by Koch and Brady.<sup>24</sup> As shown in the averaged mass-conservation equation, the average mass flux that is a linear function of the average concentration shall be written in the following form

$$\langle \mathbf{q} \rangle = (1 + \gamma) \langle \mathbf{u} \rangle \langle C \rangle - \mathbf{D} \cdot \nabla \langle C \rangle \quad (30)$$

where  $\langle \rangle$  is the sign of bulk average;  $\langle C \rangle$  is bulk average of the concentration in the porous media;  $\gamma$  is a constant that is defined by

$$\gamma = \frac{(1 - \varepsilon)(1 - m^{-1})}{1 - (1 - \varepsilon)(1 - m^{-1})} \quad (31)$$

Moreover,  $\mathbf{q}$  is the mass flux given by

$$\text{In the fluid : } \mathbf{q} = \mathbf{u}C - D_f \nabla C \quad (32a)$$

$$\text{In the particles : } \mathbf{q} = -D_p \nabla C \quad (32b)$$

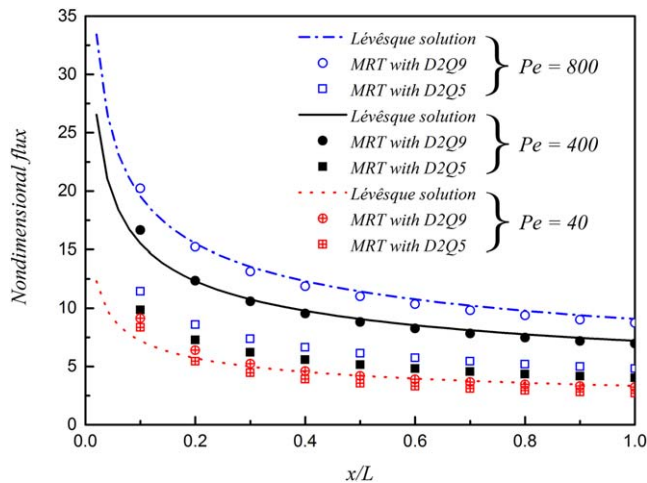


**Figure 7. Comparison of simulated mass-flux by MRT model (symbols) with the Lévêque solution (solid line).**

[Color figure can be viewed at wileyonlinelibrary.com]

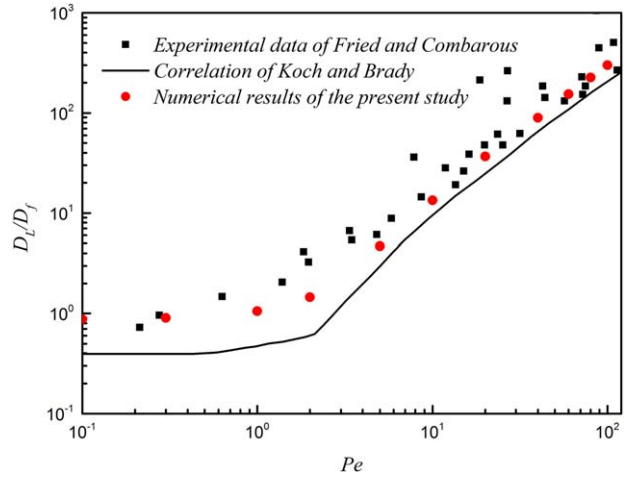


**Figure 8. Validation of the proposed LBM approach for the fixed beds with impermeable particles and  $\varepsilon = 0.5$ .**

[Color figure can be viewed at wileyonlinelibrary.com]

By substituting Eqs. 32a,b into Eq. 30, the effective diffusivity operator  $\mathbf{D}$  that is consist of tortuosity and dispersion can be obtained as follow

$$\mathbf{D} \equiv D_{\text{tor}} + \mathbf{D}_{\text{dis}} = \frac{\langle C \mathbf{u} - D \frac{\partial C}{\partial n} \rangle - (1 + \gamma) \langle \mathbf{u} \rangle \langle C \rangle}{\frac{\partial \langle C \rangle}{\partial n}} \quad (33)$$

where  $D_{\text{tor}}$  is the tortuosity factor that represents the diffusion coefficient in the interconnected pore space,  $\mathbf{D}_{\text{dis}}$  is effective dispersion operator,  $\frac{\partial C}{\partial n}$  is the concentration gradient parallel to the mass transfer direction.

To validate the LBM approach proposed in the study, the longitudinal mass dispersion calculated by the aforementioned method is compared with experimental data reported by Fried and Combarous<sup>55</sup> and the analytical correlation derived by Koch and Brady.<sup>24</sup> As experimental data were collected using impermeable particles, the comparison was conducted without the consideration of holdup dispersion, that is, no local scale diffusion inside the catalyst particles. As shown in Figure 8, it can be clearly seen that the calculated results of the present study are in good agreement with available experimental data than the analytical correlation of Koch and Brady,<sup>24</sup> especially in the range of low Péclet number. This clearly demonstrates the accuracy and robustness of the LBM approach used in this study.

## Results and Discussion

As analytically proposed by Koch and Brady,<sup>24</sup> the full form of longitudinal mass dispersion can be written as follow

$$\frac{D_L}{D_f} = \Theta_m Pe + \Theta_b Pe \ln(Pe) + \Theta_h \left( \frac{D_f}{D_p} \right)^{n_1} \left( \frac{1}{m} \right)^{n_2} Pe^2 \quad (34)$$

Note that the first term on the right side of Eq. 34 represents the mechanical contribution. Moreover, the other two terms that include boundary-layer dispersion and holdup dispersion represent the non-mechanical contribution. In Eq. 34,  $\Theta_m$ ,  $\Theta_b$ , and  $\Theta_h$  are the coefficients of three counterparts of longitudinal mass dispersion, respectively. In order to obtain a general correlation of longitudinal mass dispersion, the effect of several parameters, namely  $Pe$ ,  $\varepsilon$ ,  $m$ , and  $\frac{D_f}{D_p}$ , are investigated to



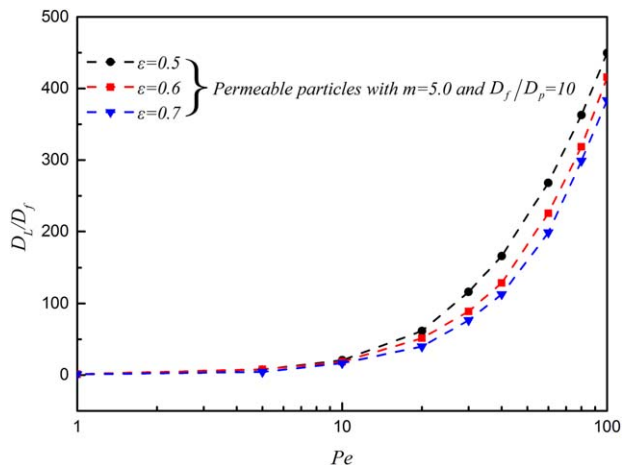


**Figure 9. Dependence of asymptotic longitudinal mass dispersion on Péclet number in fixed beds with three different porosities.**

[Color figure can be viewed at [wileyonlinelibrary.com](http://wileyonlinelibrary.com)]

determine the coefficients of three counterparts and the exponents of  $\frac{D_f}{D_p}$  and  $\frac{1}{m}$  in a wide range of porosity.

### Effect of Péclet number

In Figure 9, longitudinal mass dispersion is investigated under the variation of Péclet number. Note that porosity of fixed beds normally varies from 0.3 to 0.8 as claimed by Chuang and Wen<sup>56</sup> and Zhang et al.<sup>57</sup> Due to the limitations of RP reconstruction algorithm, it is not feasible to generate 2D porous media with randomly positioned nonoverlapping particles when porosity is lower than 0.5. Therefore, only three porosities, namely  $\varepsilon=0.5$ , 0.6 and 0.7, are considered in this study. Furthermore, reconstructed microstructures of  $\varepsilon=0.6$  and 0.7 are illustrated in Figure 10. As shown in Figure 9, it can be clearly observed that longitudinal mass dispersion increases with the rise of Péclet number (In this study,  $Pe = \frac{UL}{D}$  with  $U$  is the average velocity through the porous media and  $L$  is the particles diameter), especially in the range of  $Pe > 10$ . This is expected as previously stated for instance by Quintard and Whitaker.<sup>4</sup> The reason is that longitudinal mass dispersion is highly dependent on Péclet number. Moreover, it should be mentioned that the mechanical dispersion is proportional to  $Pe$ . For the non-mechanical dispersion, however, boundary-layer dispersion and holdup dispersion are proportional to  $Pe \ln(Pe)$  and  $Pe^2$ , respectively. As a consequence, nonmechanical dispersion overwhelms mechanical dispersion in the range of high Péclet number.

### Effect of solubility ratio

Kandhai et al.<sup>26</sup> utilized pulsed field gradient nuclear magnetic resonance (PFG-NMR) to obtain longitudinal diffusion of porous media with and without porous particles. The experimental results indicated that holdup dispersion or active dispersion, namely the rightmost term on the right side of Eq. 34, has significant influence on longitudinal mass dispersion. Therefore, solubility ratio  $m$  was investigated on longitudinal mass dispersion under the variation of Péclet number as shown in Figure 11.  $m^{-1}=0$  and  $m^{-1} \neq 0$  account for fixed beds with impermeable and permeable particles, respectively. In this subsection, four solubility ratios, namely  $m = 1.0$ , 2.0, 5.0, and 10.0, are considered. In Figure 11, it can be seen that under the same circumstance, the decrease of solubility ratio results in

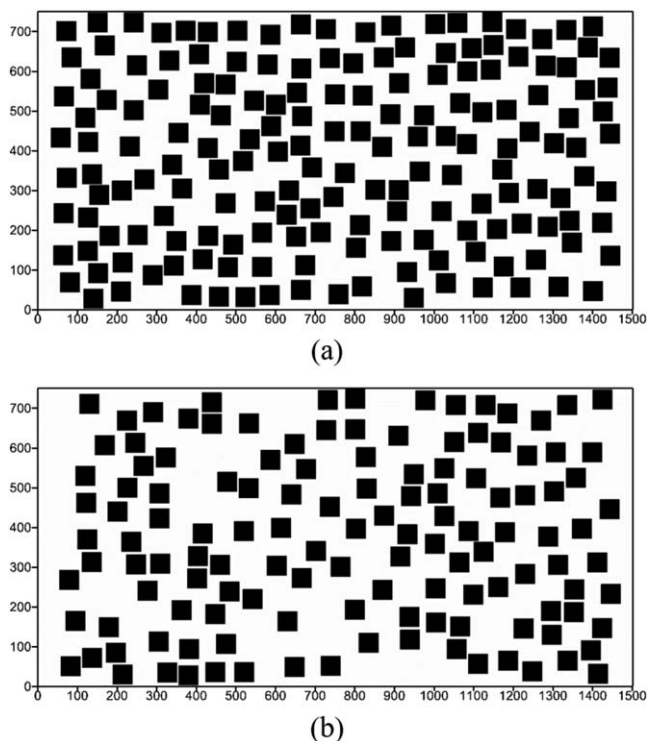


**Figure 10. Reconstructed microstructure of porous media with two different porosities: (a)  $\varepsilon=0.6$ ; (b)  $\varepsilon=0.7$ .**

the rise of longitudinal mass dispersion, which is consistent with the expression of holdup dispersion (see Eq. 34). Note that the curves of asymptotic longitudinal mass dispersion for impermeable particles are not drawn in Figure 11a,b, as the curves of  $m = 10.0$  overlap with that of impermeable particles for  $\varepsilon=0.6$  and  $\varepsilon=0.7$ .

### Effect of the ratio of molecular diffusion of solute to intraparticle diffusion

As holdup dispersion is also affected by the ratio of molecular diffusion of solute to intraparticle diffusion, the effect of the variation of  $D_f/D_p$  on longitudinal mass dispersion was investigated in Figure 12. Yoshida and Takatsuji<sup>58</sup> experimentally measured intraparticle diffusion coefficients of acetic acid and lactic acid in a weakly basic ion exchanger. The experimental results show that  $D_f/D_p$  normally varies from 1 to 10. Three ratios, namely  $D_f/D_p=2$ , 5 and 10, are considered in the study. As pointed out by Maier et al.,<sup>25</sup> holdup dispersion mainly results from several factors, such as dead-end pores, recirculation cells, and other regions of zero fluid velocity. Therefore, it is expected that the decrease of intraparticle diffusion results in the intensification of longitudinal mass dispersion, which is consistent with the trend found in Figure 12. It is also possible to correlate this with Eq. 34, where the last term of the equation deals with this ratio. As the ratio  $D_f/D_p$  increases, the holdup dispersion increases.

### Correlation of longitudinal mass dispersion

Longitudinal mass dispersion plays an important role in predicting the macroscopic mass transport characteristics of solute in porous media. However, the available correlations of longitudinal mass dispersion are only valid in a specific range

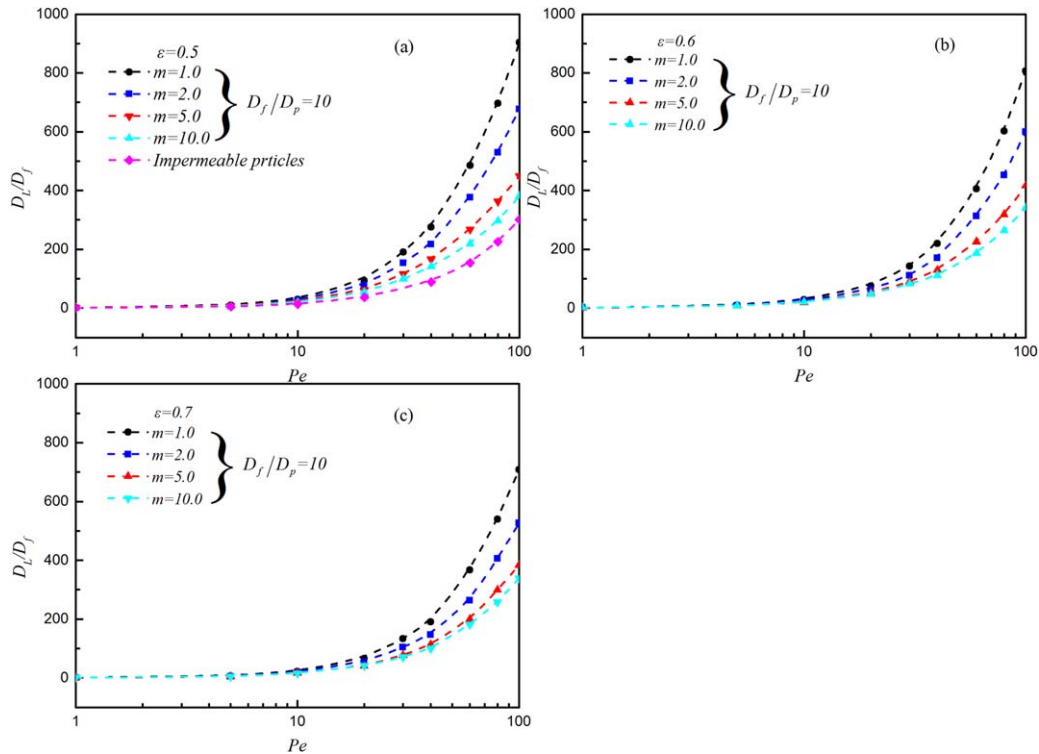


**Figure 11. Dependence of asymptotic longitudinal mass dispersion on the solubility ratio  $m$  in fixed beds: (a)  $\varepsilon=0.5$ ; (b)  $\varepsilon=0.6$ ; (c)  $\varepsilon=0.7$ .**

[Color figure can be viewed at [wileyonlinelibrary.com](http://wileyonlinelibrary.com)]

of porosity. Thus, a general correlation that can be applied in a wide range of porosity is highly needed.

Based on the investigations of several parameters in Eq. 34, namely, Péclet number, porosity, solubility ratio, and ratio of molecular diffusion of solute to intraparticle diffusion, a new

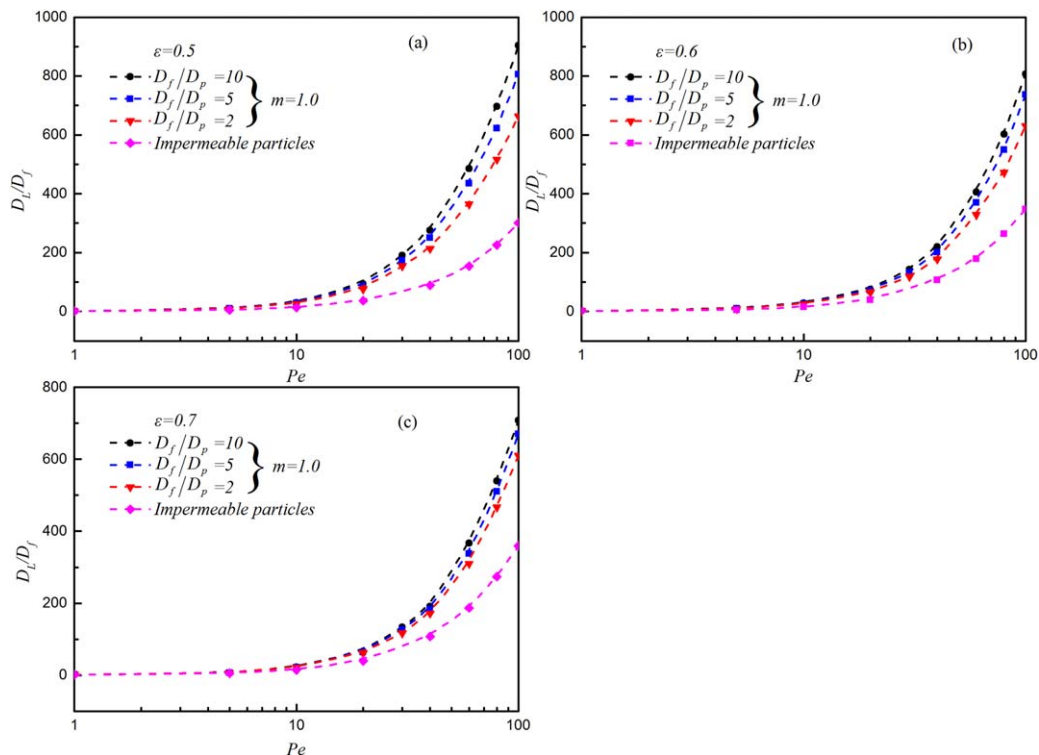


**Figure 12. Dependence of asymptotic longitudinal mass dispersion on the ratio of molecular diffusion of solute to intraparticle diffusion in fixed beds: (a)  $\varepsilon=0.5$ ; (b)  $\varepsilon=0.6$ ; (c)  $\varepsilon=0.7$ .**

[Color figure can be viewed at [wileyonlinelibrary.com](http://wileyonlinelibrary.com)]

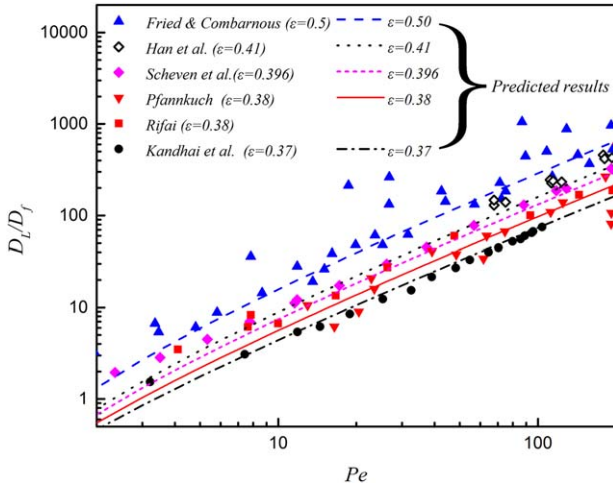


**Figure 13.** Comparison of the predicted results (solid lines) from the proposed correlation with experimental data of longitudinal mass dispersion without the consideration of holdup dispersion (experimental data of  $\varepsilon=0.37$  obtained by magnetic resonance imaging by Kandhai et al.<sup>26</sup> (•),  $\varepsilon=0.38$  (Rifai et al.,<sup>59</sup> Pfannkuch<sup>60</sup>) (■, ▼),  $\varepsilon=0.396$  (Scheven et al.<sup>61</sup>) (◆),  $\varepsilon=0.41$  (Han et al.<sup>62</sup>) (◇) and  $\varepsilon=0.5$  (Fried and Combarnous<sup>55</sup>) (▲)).

[Color figure can be viewed at wileyonlinelibrary.com]

correlation was proposed. In regard to Eq. 34, the values of the parameters ( $\Theta_m$ ,  $\Theta_b$ ,  $\Theta_h$ ),  $n_1$ , and  $n_2$  were obtained by the least-square method and presented as follows

$$\Theta_m = (1.110 \pm 0.0268) \cdot \varepsilon^2 - (0.00976 \pm 0.00101) \quad (35)$$

$$\Theta_b = [(3.099 \pm 0.312) \cdot \ln(\varepsilon) + (3.287 \pm 0.168)] \cdot (1 - \varepsilon) \quad (36)$$

$$\Theta_h = (0.00868 \pm 3.075 \times 10^{-6}) / \varepsilon^2 + (0.00852 \pm 9.374 \times 10^{-6}) \quad (37)$$

$$n_1 = 0.241 \quad (38)$$

$$n_2 = 0.950 \quad (39)$$

To validate the accuracy of the proposed correlation, two comparisons are conducted by comparing the predicted results with available experimental data found in the literature. As holdup dispersion is hard to detect in experimental measurements, most of data associated with longitudinal mass dispersion just include mechanical dispersion and boundary-layer dispersion. As shown in Figure 13, a comparison of the predicted results from the proposed correlation with experimental data of longitudinal mass dispersion that only includes mechanical dispersion and boundary-layer dispersion is conducted under the variation of porosity. From this figure, it can be found that the correlation is established based on the numerical results of  $\varepsilon=0.5$ , 0.6, and 0.7, but the predicted results of the proposed correlation are in good agreement with experimental data of  $\varepsilon=0.37$  from Kandhai et al.,<sup>26</sup>  $\varepsilon=0.38$  from Rifai et al.<sup>59</sup> and Pfannkuch,<sup>60</sup>  $\varepsilon=0.396$  from Scheven et al.,<sup>61</sup>  $\varepsilon=0.41$  from Han et al.<sup>62</sup> and  $\varepsilon=0.5$  from Fried and Combarnous.<sup>55</sup> Moreover, it should be mentioned that experimental data of Kandhai et al.<sup>26</sup> and Scheven et al.<sup>61</sup> were obtained by conducting NMR spectroscopy experiments. Nevertheless, Rifai et al.,<sup>59</sup> Pfannkuch et al.<sup>60</sup> and Fried and Combarnous<sup>55</sup> utilized step function method and H<sub>2</sub>O-NaCl system to achieve experimental data of mass dispersion.

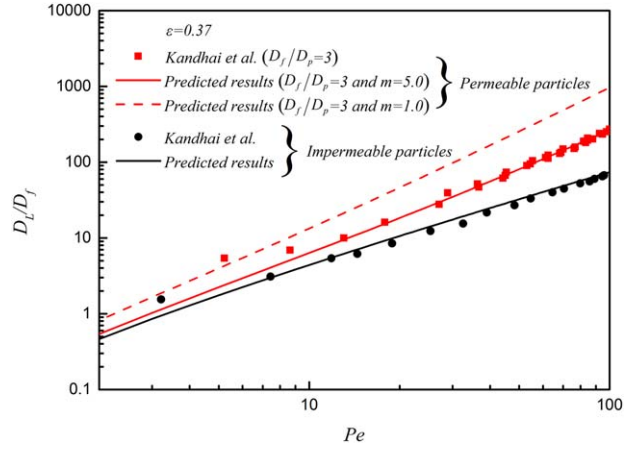


**Figure 14.** Comparison of the predicted results from the proposed correlation with experimental data of longitudinal mass dispersion (experimental data of  $\varepsilon=0.37$  obtained by magnetic resonance imaging by Kandhai et al.<sup>26</sup>).

[Color figure can be viewed at wileyonlinelibrary.com]

More details related to experimental methods on mass dispersion of liquids in packed beds can be found in the excellent reference by Delgado.<sup>63</sup>

As the previous comparison did not consider the contribution of holdup dispersion, further comparison is conducted using the limited experimental data from Kandhai et al.,<sup>26</sup> which measured longitudinal mass dispersion of fixed beds with and without porous particles. As illustrated in Figure 14, the predicted results of the proposed correlation and experimental data are plotted against the variation of Péclet number. Note that the evident difference between experimental data of impermeable particles and permeable particles represents the importance of holdup dispersion. For impermeable particles, the agreement between the correlation and experimental data has already been discussed. As solubility ratio  $m$  cannot be found in experimental data of Kandhai et al.,<sup>26</sup> the predicted results in the solubility ratio  $m$  range from 1 to infinity are compared with experimental data with permeable particles. It has been found that better agreement can be achieved for the case of  $m=5$ . Therefore, if one wants to use the proposed correlation to predict the longitudinal mass dispersion of fixed bed with permeable particles, an appropriate value of  $m$  should be determined in advance.

Then, the proposed correlations in the present study, namely Eqs. 35–39, are valid for fixed beds with randomly positioned impermeable and permeable particles in the porosity range from 0.3 to 0.7.

## Conclusions

In this study, numerical simulations using LBM approach were performed to calculate asymptotic longitudinal mass dispersion of porous media with permeable particles. Moreover, a 2-D microstructure of porous media was generated by random placement (RP) algorithm. Based on the results achieved in this study, three remarks can be sorted as follows:

1. A LBM approach was applied to investigate the fluid flow and mass transfer characteristics of solute in porous media with randomly positioned particles. In the approach, a D2Q9 model with multi-relaxation-time (MRT) collision operator that is appropriate for incompressible flow with a

high Péclet number without refining the lattice was chosen after a cross comparison with an available test case.

2. Several parameters, which are  $Pe$ ,  $\varepsilon$ ,  $m$ , and  $D_f/D_p$ , were investigated on the influence of asymptotic longitudinal mass dispersion. It has been found that in the range of high Péclet number, non-mechanical dispersion is more dominant than mechanical dispersion.

3. A new correlation of longitudinal mass dispersion was established. By comparing the predicted results with available experimental data in the literature, it has been found that the prediction of longitudinal mass dispersion is acceptable in a wide range of porosity, indicating the validity of the proposed correlation.

As evidence, this clearly demonstrates the accuracy of the LBM approach to deal with complex phenomena in porous media, including active dispersion. As a next step, complex reactivity could be easily included to investigate their effects on effective mass dispersion and compare the results with available theoretical works like the one of Whitaker<sup>3</sup> for instance. This could be done in complex geometries, eventually in 3-D.

## Acknowledgments

The authors would like to express their sincere thanks to the National Natural Science Foundation of China (Project No. 91534106 and 21506032), Distinguished Young Researcher Training Project in Universities of Fujian Province (Project No. 83016023), Fuzhou University Qishan Scholar (Overseas Project) (Project No. XRC-1458) and 111 Project (Project No. D17005) for financially supporting this study.

## Notation

$c_s$  = lattice sound speed, m/s  
 $C$  = solute concentration, mol/m<sup>3</sup>  
 $D$  = diffusivity, m<sup>2</sup>/s  
 $e_i$  = discrete velocity, m/s  
 $f$  = distribution function for fluid flow  
 $g$  = distribution function for mass transfer  
 $Q$  = steady-state normalized mass flux  
 $K$  = Henry's law constant in Eq. 28  
 $L$  = characteristic length in Eq. 18, m  
 $m$  = ratio of the solubilities of the solute in the fluid and in the catalyst particles  
 $Ma$  = Mach number  
 $\mathbf{M}$  = transformation matrix  
 $\mathbf{n}$  = normal unit vector from the catalyst particle surface to the fluid  
 $p$  = pressure, Pa  
 $Pe$  = Péclet number  
 $\mathbf{q}$  = mass flux, mol/m<sup>2</sup> s  
 $s_i$  = parameters in the relaxation matrix in Eq. 13  
 $\mathbf{S}_f$  = diagonal relaxation matrix for fluid flow  
 $\mathbf{S}_g$  = diagonal relaxation matrix for mass transfer  
 $t$  = time, s  
 $\mathbf{u}$  = fluid velocity tensor, m/s  
 $U$  = characteristic velocity in Eq. 18, m/s  
 $V$  = volume, m<sup>3</sup>  
 $w_i$  = weight coefficient  
 $\mathbf{x}$  = position tensor, m  
 $x$  = horizontal coordinate, m  
 $y$  = vertical coordinate, m

## Greek letters

$\varepsilon$  = porosity  
 $\gamma$  = constant in Eq. 30 and defined by Eq. 31  
 $\rho$  = density, kg/m<sup>3</sup>  
 $\sigma$  = viscous stress tensor, Pa  
 $\Omega$  = collision operator

$\tau$  = relaxation time  
 $\nu$  = kinematic viscosity, m<sup>2</sup>/s  
 $\lambda_i$  = parameters in the relaxation matrix in Eq. 21  
 $\Theta$  = coefficients in Eq. 34

## Special symbols

$\langle \rangle$  = bulk average  
 $*$  = post-collision

## Subscripts and superscripts

$b$  = boundary-layer  
 $dis$  = dispersion  
 $eq$  = equilibrium  
 $f$  = fluid  
 $h$  = holdup  
 $in$  = in the catalyst particles  
 $L$  = longitudinal mass dispersion  
 $m$  = mechanical  
 $n_1, n_2$  = exponents in Eq. 34  
 $out$  = in the void of porous media  
 $p$  = pore  
 $tor$  = tortuosity

## Literature Cited

- Cheng P. Heat transfer in geothermal systems. *Adv Heat Transf.* 1979;14:1–105.
- Nakayama A. Convective flows in porous media. In: *PC-Aided Numerical Heat Transfer and Convective Flow*. Boca Raton, New York: CRC Press, 1995:103–176.
- Whitaker S. *The Method of Volume Averaging*. Boston: Springer, 1999.
- Quintard M, Whitaker S. Convection, dispersion, and interfacial transport of contaminants: Homogeneous porous media. *Adv Water Res.* 1994;17(4):221–239.
- Quintard M, Bletzacker L, Chenu D, Whitaker S. Nonlinear, multi-component, mass transport in porous media. *Chem Eng Sci.* 2006; 61(8):2643–2669.
- Yang C, Nakayama A. A synthesis of tortuosity and dispersion in effective thermal conductivity of porous media. *Int J Heat Mass Transf.* 2010;53(15–16):3222–3230.
- Masoodi R, Tan H, Pillai KM. Darcy's law-based numerical simulation for modeling 3D liquid absorption into porous wicks. *AIChE J.* 2011;57(5):1132–1143.
- Perré P, Turner IW. A dual-scale model for describing drier and porous medium interactions. *AIChE J.* 2006;52(9):3109–3117.
- Yang C, Thovert JF, Debenest G. Upscaling of mass and thermal transports in porous media with heterogeneous combustion reactions. *Int J Heat Mass Transf.* 2015;84:862–875.
- Yang C, Wang QL, Guo JD, Nakayama A, Qiu T. Upscaling solute concentration transport equations of countercurrent dialyzer systems. *Chem Eng Sci.* 2015;134:108–118.
- Qiu T, Wang QL, Yang C. Upscaling multicomponent transport in porous media with a linear reversible heterogeneous reaction. *Chem Eng Sci.* 2017;171:100–116.
- Chai ZH, Huang CS, Shi BC, Guo ZL. A comparative study on the lattice Boltzmann models for predicting effective diffusivity of porous media. *Int J Heat Mass Transf.* 2016;98:687–696.
- Chukwudozie C, Tyagi M. Pore scale inertial flow simulations in 3-D smooth and rough sphere packs using lattice Boltzmann method. *AIChE J.* 2013;59(12):4858–4870.
- Zhang LZ. A lattice Boltzmann simulation of mass transport through composite membranes. *AIChE J.* 2014;60(11):3925–3938.
- Zhou L, Qu ZG, Chen L, Tao WQ. Lattice Boltzmann simulation of gas–solid adsorption processes at pore scale level. *J Comput Phys.* 2015;300:800–813.
- Zhou L, Qu ZG, Ding T, Miao JY. Lattice Boltzmann simulation of the gas–solid adsorption process in reconstructed random porous media. *Phys Rev E.* 2016;93(4):043101
- Pan ZH, Zhao CY. Prediction of the effective thermal conductivity of packed bed with micro-particles for thermochemical heat storage. *Sci Bulletin.* 2016;62:256–265.
- Yan XH, Li N. Simulation of solute dispersion in particle packs by the volume averaging method. *Comput Chem Eng.* 2017;98:154–160.

19. Li X, Zhang Y, Wang X, Ge W. GPU-based numerical simulation of multi-phase flow in porous media using multiple-relaxation-time lattice Boltzmann method. *Chem Eng Sci.* 2013;102:209–219.
  20. Hu Y, Li D, Shu S, Niu X. A multiple-relaxation-time lattice Boltzmann model for the flow and heat transfer in a hydrodynamically and thermally anisotropic porous medium. *Int J Heat Mass Transf.* 2017;104:544–558.
  21. Wang DD, Liu ZC, Shen J, Liu W. Lattice Boltzmann simulation of effective thermal conductivity of porous media with multiphase. *J Porous Media.* 2015;18(10):929–939.
  22. Wang M, Wang J, Pan N, Chen S. Mesoscopic predictions of the effective thermal conductivity for microscale random porous media. *Phys Rev E.* 2007;75(3):036702
  23. Hussain M, Tian E, Cao TF, Tao WQ. Pore-scale modeling of effective diffusion coefficient of building materials. *Int J Heat Mass Transf.* 2015;90:1266–1274.
  24. Koch DL, Brady JF. Dispersion in fixed beds. *J Fluid Mech.* 1985; 154(1):399–427.
  25. Maier RS, Kroll DM, Bernard RS, Howington SE, Peters JF, Davis HT. Pore-scale simulation of dispersion. *Phys Fluids.* 2000;12(8): 2065–2079.
  26. Kandhai D, Hlushkou D, Hoekstra AG, Sloot PM, Van As H, Tallarek U. Influence of stagnant zones on transient and asymptotic dispersion in macroscopically homogeneous porous media. *Phys Rev Lett.* 2002;88(23):234501
  27. Succi S, Karlin IV, Chen H. Colloquium: Role of the H theorem in lattice Boltzmann hydrodynamic simulations. *Rev Modern Phys.* 2002;74(4):1203
  28. Ansumali S, Karlin IV, Öttinger HC. Minimal entropic kinetic models for hydrodynamics. *EPL (Europhys Lett).* 2003;63(6):798–804.
  29. Huber C, Chopard B, Manga M. A lattice Boltzmann model for coupled diffusion. *J Comput Phys.* 2010;229(20):7956–7976.
  30. Yang X, Shi B, Chai Z. Coupled lattice Boltzmann method for generalized Keller–Segel chemotaxis model. *Comput Math Appl.* 2014; 68(12):1653–1670.
  31. Ginzburg I. Equilibrium-type and link-type lattice Boltzmann models for generic advection and anisotropic-dispersion equation. *Adv Water Res.* 2005;28(11):1171–1195.
  32. Servan-Camas B, Tsai FTC. Lattice Boltzmann method with two relaxation times for advection–diffusion equation: third order analysis and stability analysis. *Adv Water Res.* 2008;31(8):1113–1126.
  33. Lallemand P, Luo LS. Theory of the lattice Boltzmann method: dispersion, dissipation, isotropy, Galilean invariance, and stability. *Phys Rev E.* 2000;61(6):6546
  34. Luo LS, Liao W, Chen X, Peng Y, Zhang W. Numerics of the lattice Boltzmann method: effects of collision models on the lattice Boltzmann simulations. *Phys Rev E.* 2011;83(5):056710
  35. He X, Luo LS. Lattice Boltzmann model for the incompressible Navier–Stokes equation. *J Stat Phys.* 1997;88(3):927–944.
  36. Bettaibi S, Kuznik F, Sediki E. Hybrid LBM-MRT model coupled with finite difference method for double-diffusive mixed convection in rectangular enclosure with insulated moving lid. *Phys A Stat Mech Appl.* 2016;444:311–326.
  37. Holme R, Rothman DH. Lattice-gas and lattice-Boltzmann models of miscible fluids. *J Stat Phys.* 1992;68(3–4):409–429.
  38. Sterling JD, Chen S. Stability analysis of lattice Boltzmann methods. *J Comput Phys.* 1996;123(1):196–206.
  39. Rakotomalala N, Salin D, Watzky P. Miscible displacement between two parallel plates: BGK lattice gas simulations. *J Fluid Mech.* 1997;338:277–297.
  40. Leconte M, Martin J, Rakotomalala N, Salin D. Pattern of reaction diffusion fronts in laminar flows. *Phys Rev Lett.* 2003;90(12):128302
  41. Meng XH, Guo ZL. Multiple-relaxation-time lattice Boltzmann model for incompressible miscible flow with large viscosity ratio and high Péclet number. *Phys Rev E.* 2015;92(4):043305
  42. Succi S. *The Lattice Boltzmann Equation for Fluid Dynamics and Beyond.* Oxford, UK: Oxford University Press, 2001.
  43. Guo ZL, Zheng CG, Shi BC. Non-equilibrium extrapolation method for velocity and pressure boundary conditions in the lattice Boltzmann method. *Chin Phys.* 2002;11(4):366–374.
  44. Kang Q, Lichtner PC, Zhang D. Lattice boltzmann pore-scale model for multicomponent reactive transport in porous media. *J Geophys Res Solid Earth.* 2006;111(B5):1–9.
  45. Kang QJ, Lichtner PC, Zhang DX. An improved lattice Boltzmann model for multicomponent reactive transport in porous media at the pore scale. *Water Res Res.* 2007;43(12):1–12.
  46. Yang C, Mao ZS. Numerical simulation of interphase mass transfer with the level set approach. *Chem Eng Sci.* 2005;60(10):2643–2660.
  47. Johns ML, Sederman AJ, Bramley AS, Gladden LF, Alexander P. Local transitions in flow phenomena through packed beds identified by MRI. *AIChE J.* 2000;46(11):2151–2161.
  48. Robbins DJ, El-Bachir MS, Gladden LF, Cant RS, von Harbou E. CFD modeling of single-phase flow in a packed bed with MRI validation. *AIChE J.* 2012;58(12):3904–3915.
  49. Guibert R, Nazarova M, Horgue P, Hamon G, Creux P, Debenest G. Computational permeability determination from pore-scale imaging: sample size, mesh and method sensitivities. *Transport Porous Media.* 2015;107(3):641–656.
  50. Adler PM, Thovert JF. Real porous media: local geometry and macroscopic properties. *Appl Mech Rev.* 1998;51(9):537–585.
  51. Yazdchi K, Srivastava S, Luding S. Micro–macro relations for flow through random arrays of cylinders. *Compos Part A Appl Sci Manuf.* 2012;43(11):2007–2020.
  52. Khirevich S, Daneyko A, Hölzel A, Seidel-Morgenstern A, Tallarek U. Statistical analysis of packed beds, the origin of short-range disorder, and its impact on eddy dispersion. *J Chromatog A.* 2010; 1217(28):4713–4722.
  53. Lévêque A. Les lois de la transmission de chaleur par convection. *Ann Des Mines.* 1928;13:201–239.
  54. Machado R. Numerical simulations of surface reaction in porous media with lattice Boltzmann. *Chem Eng Sci.* 2012;69(1):628–643.
  55. Fried JJ, Combarous MA. Dispersion in porous media. *Adv Hydrosci* 1971;7:169–282.
  56. Chung SF, Wen CY. Longitudinal dispersion of liquid flowing through fixed and fluidized beds. *AIChE J.* 1968;14(6):857–866.
  57. Zhang WL, Thompson KE, Reed AH, Beenken L. Relationship between packing structure and porosity in fixed beds of equilateral cylindrical particles. *Chem Eng Sci.* 2006;61(24):8060–8074.
  58. Yoshida H, Takatsuji W. Parallel transport of an organic acid by solid-phase and macropore diffusion in a weakly basic ion exchanger. *Ind Eng Chem Res.* 2000;39(4):1074–1079.
  59. Rifai MNE, Kaufman WJ, Todd DK. Dispersion phenomena in laminar flow through porous media. Sanitary Engineering Research Laboratory and Division of Civil Engineering, University of California, Berkeley, CA, 1956;90:157.
  60. Pfannkuch HO. Contribution - l'étude des déplacements de fluides miscibles dans un milieu poreux. *Revue De L'institut Francais Du Petrole* 1963;18:1–54.
  61. Scheven UM, Khirevich S, Daneyko A, Tallarek U. Longitudinal and transverse dispersion in flow through random packings of spheres: a quantitative comparison of experiments, simulations, and models. *Phys Rev E.* 2014;89(5):053023
  62. Han NW, Bhakta J, Carbonell RG. Longitudinal and lateral dispersion in packed beds: effect of column length and particle size distribution. *AIChE J.* 1985;31(2):277–288.
  63. Delgado JMPQ. A critical review of dispersion in packed beds. *Heat Mass Transf.* 2006;42(4):279–310.
-